ELSEVIER

Colloids and Surfaces
A: Physicochemical and Engineering Aspects 155 (1999) 259–276

COLLOIDS AND SURFACES A

www.elsevier.nl/locate/colsurfa

Three-phase flow and wetability effects in triangular capillaries

Tuba Firincioglu [a], Martin J. Blunt [a,*], Dengen Zhou [b]

[a] *Department of Petroleum Engineering, Stanford University, Stanford, CA 94305-2220, USA*
[b] *Chevron 1300 Beach Blvd. PO Box 446, La Habra, CA 90633-0446, USA*

Received 9 July 1998; accepted 20 January 1999

Abstract

We performed a series of two and three-phase flow experiments in capillary tubes with equilateral triangular cross-sections. We measured the flow rates of oil and water in water-wet tubes and compared them with predictions using an empirical theoretical expression for fluid conductance. Our results are consistent with a free boundary condition at the gas/liquid interface, and with a no-flow boundary at the oil/water interface, when water is stationary, and a condition between a no-flow and a free-boundary when oil and water flow simultaneously. By studying oils with different spreading coefficients we measured the circumstances when oil layers form, and we compared the results with a simple geometric argument for oil layer existence. We also studied flow in uniformly oil-wet tubes. Overall, the work verifies and calibrates theoretical expressions for fluid conductance and layer formation that can be inputted into pore level network models to predict macroscopic properties, such as relative permeability. We illustrated this approach by using our work to interpret three-phase relative permeability experiments on sandpacks.

Keywords: Capillarity; Corner flow; Spreading; Three-phase flow; Wetability

1. Introduction

The flow of the three phases—oil, water and gas—in porous media occurs in a variety of different circumstances, including pollutant transport in the unsaturated zone, and gas injection in oil reservoirs. A quantitative understanding of three-phase flow is necessary to predict contaminant movement and clean up, and oil recovery by gas flooding. Relative permeability and capillary pressure are empirical macroscopic parameters used to describe multiphase flow in porous media [1]. Despite the development of empirical functional forms for three-phase relative permeability [2] and a growing body of experimental data, see for instance Oak [3] and Jerauld [4], the subject lacks a fundamental basis grounded on an understanding of the configuration of three phases at the pore scale and their flow rates.

* Corresponding author. Tel.: +1-650-7252727; fax: +1-650-7252099.
E-mail address: blunt@pangea.stanford.edu (M.J. Blunt)

0927-7757/99/$ - see front matter
PII: S0927-7757(99)00039-4

Gravity drainage, or the downwards movement of oil and water in the presence of gas, is a common three-phase displacement occurring in, for instance, the migration of non aqueous phase pollutants towards the water table, or gas cap expansion in an oil reservoir. Several experimental studies have shown that three-phase gravity drainage can lead to very high oil recoveries in water-wet media [5–7]. Micromodel studies that visualize the fluid flow on the pore scale have shown that the mechanism for high oil recovery is slow drainage through oil layers [8–12]. Several three-phase pore level network models have been developed that incorporate the displacement processes seen in micromodels [13–17]. These network models can predict three-phase relative permeability based on the physics at the pore scale. However, the use of network modeling to provide a quantitative understanding of three-phase flow is faced with two major problems. First, micromodel experiments do not directly measure fluid conductance at the pore scale, on which a prediction of relative permeability from network modeling is based. The computed relative permeabilities are sensitive to the expressions used for fluid conductance and the boundary conditions assumed between the phases, particularly for the prediction of oil relative permeability at low oil saturation, which is exactly the regime of greatest interest in the understanding of three-phase gravity drainage [13,14]. Second, while the majority of studies, both numerical and experimental, have been performed for water-wet media, most oil reservoirs are either oil-wet or display characteristics between the water-wet and oil-wet extremes [4]. Despite some work on oil-wet systems [18–20], we are far from a fundamental understanding of the effect of wetability in three-phase flow.

In this paper we perform a series of experiments in triangular capillary tubes to measure oil and water flow rates during gravity drainage. We study the effect of fluid properties and wetability, and compare the results with empirical theoretical expressions for fluid conductance. While these expressions involve some approximations, they provide a convenient mathematical form for input into network modeling. The purpose of this work is to obtain a quantitative understanding of three-phase flow in a single capillary suitable for input into predictive pore scale models. A similar approach has already been pursued for two-phase flow [21]: triangular capillaries represented the pore space and approximate analytical formulae were used to find conductances. By this method relative permeabilities for two-phase flow were successfully predicted. Our work provides a basis for similar studies of three-phase flow.

Zhou et al. [22], derived approximate expressions for fluid conductance and compared the results with finite element solutions for corner flow [23] and with experiments conducted in square capillaries. We extend the work of Zhou et al. [22]. First we study situations where both oil and water are flowing simultaneously. Second we measure the circumstances under which a layer of oil forms in the pore space. Third we investigate flow in uniformly oil-wet tubes.

2. Basic concepts

2.1. Pore geometry and layers

The configuration of the fluids in the pore space is determined by the interfacial tensions of the fluids, the rock wetability and capillary pressure [24,13]. An important geometric characteristic of a pore is the corners and crevices that it has. To represent this feature we study flow in non-circular capillaries rather than in circular ones. The comparison of circular and non-circular capillaries with two phases present can be seen in Fig. 1. In both cases the non-wetting phase occupies the center of the pore space. The main difference occurs in the flow mechanism of the wetting phase. In circular capillaries the wetting phase

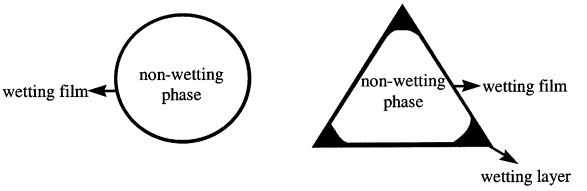

Fig. 1. Comparison of circular and non-circular capillaries.

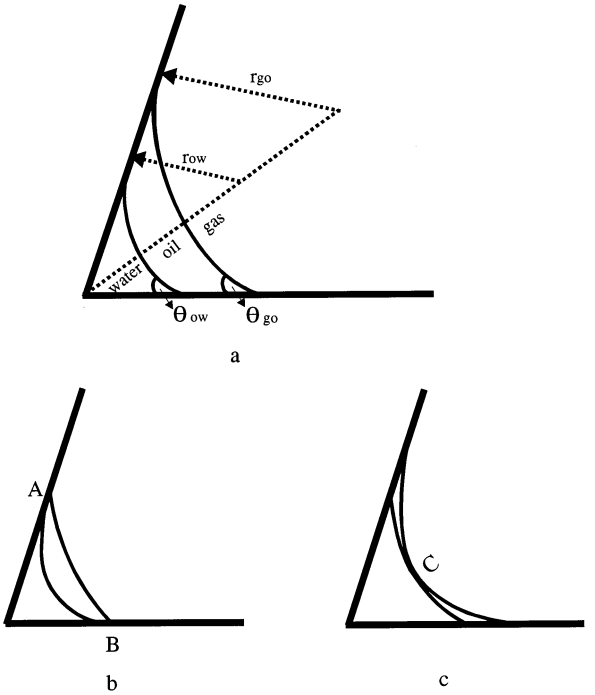

Fig. 2. The configuration of three phases in a water-wet corner. (a) Layer flow. (b) When $\theta_{go} > \theta_{ow}$ the gas–oil and oil–water interfaces meet at points A–B. (c) When $\theta_{ow} > \theta_{go}$ the gas–oil and oil–water interfaces meet at point C.

flows in thin films formed on the surface of the capillary, while in a non-circular capillary this flow mainly occurs through the layers formed in the corners. It is possible to form layers with a thickness of several microns in triangular tubes, which are much thicker than the thin films in circular capillaries that are in order of nanometers across and through which the flow rates are negligible [25].

With three-phases present in a water-wet porous medium, oil may form a layer in the pore space wedged between a wetting layer of water in the corner and gas in the center, as shown in Fig. 2. It is drainage through oil layers that is responsible for the high oil recoveries seen experimentally [13].

Several authors have hypothesized that high oil recoveries during gas injection are related to the spreading coefficient for oil [5], [20]:

$$C_{so} = \gamma_{gw} - \gamma_{ow} - \gamma_{go} \quad (1)$$

where γ_{gw}, γ_{ow}, γ_{go} are the gas/water, oil/water and gas/oil interfacial tensions, respectively. Spreading coefficients are calculated by using either the interfacial tensions measured when the fluids first contacted each other or when the three fluids are in thermodynamic equilibrium. In this study the superscript i is used to denote initial conditions.

Table 1 shows a comparison of the residual oil saturation S_{or} after gas injection for spreading ($C_{so}^{i} > 0$) and non-spreading ($C_{so}^{i} < 0$) oils. While spreading systems tend to give higher recovery, there is not a clear relation between S_{or} and C_{so}^{i}. The hypothesis proposed by several authors such as Dumoré & Schols [5] and Vizika & Lombard [20], that only spreading oils can form layers in the pore space, resulting in high oil recoveries,

Table 1
Experimental recoveries for spreading and non-spreading systems in water-wet media

References	Residual oil saturation (S_{or})%	
	Spreading ($C_s^i > 0$)	Non-spreading ($C_s^i < 0$)
Catalan et al. [26] (bead packs)	2.0	16.9
Catalan et al. [26] (Berea sandstone)	11.5–14.9	–
Dumoré & Schols [5] (sandstone)	2.9	3.2
Kalaydijan et al. [27] (Clashach sandstone)	10	31
Kalaydijan et al. [27] (Fountainbleu sandstone)	16	20
Kantzas et al. [7] (bead packs)	0.6–9.1	–
Skurdal et al. [28] (sandstone)	4.7	6.7
Vizika [29] (sandpacks)	11	23
Zhou and Blunt [6] (sandpacks)	0.13–1.49	0.35–5.25

cannot explain the low values of S_{or} seen for $C^{i}_{so} < 0$. This result is explained by noting that oil layers can form for non-spreading oils. The arrangement of fluids is actually controlled by the contact angles, wetability and capillary pressures [14]. Oil layers have indeed been observed directly in micromodels for systems with $C^{i}_{so} < 0$ [10], [12].

Fenwick and Blunt [13] used a simple geometric argument to study oil layer formation. In Fig. 2(a), an oil layer may form if;

$$\theta_{go} + \alpha < \frac{\pi}{2} \tag{2}$$

and

$$\theta_{ow} + \alpha < \frac{\pi}{2} \tag{3}$$

where, α is the half angle of the corner ($\pi/6 = 30°$ for an equilateral triangle) and θ_{go} and θ_{ow} are gas/oil and oil/water contact angles, respectively. An oil layer exists between gas and water as long as the oil/water and gas/oil interfaces do not meet. The ratio of the radius of curvatures can be defined as follows:

$$R = r_{ow}/r_{go} \tag{4}$$

here, r_{ow} is the radius of curvature of the oil/water interface and r_{go} is the radius of curvature of the gas/oil interface.

Fenwick and Blunt [13] defined a critical ratio R_c which is the ratio of radius of curvatures when the interfaces first meet. When $R > R_c$ layers are absent, and layers are formed when $R \leq R_c$. The formation of layers is not directly related to spreading coefficient, but depends on R, the corner geometry and the contact angles. They derived the following expression for the critical radius of curvature ratio assuming that $\theta_{go} \geq \theta_{ow}$ and the interfaces meet at points A and B (Fig. 2b):

$$R_c = \frac{\cos(\theta_{go} + \alpha)}{\cos(\theta_{ow} + \alpha)} \tag{5}$$

We use the same idea is used to find an expression for R_c when $\theta_{ow} > \theta_{go}$. In this case the interfaces meet in the middle at point C (Fig. 2c) and by using simple geometry, R_c is:

$$R_c = \frac{\cos(\theta_{go} + \alpha) - \tan\alpha + \tan\alpha\,\sin(\theta_{go} + \alpha)}{\cos(\theta_{ow} + \alpha) - \tan\alpha + \tan\alpha\,\sin(\theta_{ow} + \alpha)} \tag{6}$$

2.2. Layer conductance

There have been several studies that investigate layer flow in porous media. Ransohoff and Radke [23] solved the Navier–Stokes equation numerically for two-phase flow, where oil flowed in the corner and gas filled the rest of the system. They defined a dimensionless resistance β;

$$\beta = \frac{r^2_{go} A_{cor}(-\nabla\Phi)}{\mu_o q_o} \tag{7}$$

where, $\nabla\Phi$ is the potential gradient, μ_o is viscosity of oil, A_{cor} is the area of one corner and q_o is the oil flow rate through one corner (volume per unit time). Ransohoff and Radke [23] tabulated β as a function of interfacial boundary conditions, contact angle and corner geometry. In this work β is used as a tool to analyze the experimental results for both two and three-phase flow.

Lenormand and Zarcone [30] used a hydraulic diameter approximation to calculate the imbibition rate of water into gas in square capillaries. The thin film approach was used by Blunt et al. [25] to estimate the oil drainage rates in three-phase flow.

Recently, Zhou et al. [22] proposed another approximation to compute oil flow in a three-phase system, shown in Fig. 2. They assumed thin film flow, with an effective film thickness proportional to the ratio of the flow area to the length of no-flow boundary. The dimensionless resistance β is:

$$\beta = \frac{12\sin^2\alpha(1-B)^2(\psi_1 - B\psi_2)(\psi_3 + f_2 B\psi_2 - (1-f_1 B)R)^2}{(1-\sin\alpha)^2 B^2(\psi_1 - B\psi_2 - (1-B)R^2)^3} \tag{8a}$$

$$\psi_1 = \cos^2(\alpha + \theta_{go}) + \cos(\alpha + \theta_{go})\sin(\alpha + \theta_{go})\tan\alpha \tag{8b}$$

$$\psi_2 = 1 - \frac{\theta_{go}}{\pi/2 - \alpha}$$

Table 2
Contact angles and interfacial tensions of the oils used in the experiments[a]

	θ_{ow} (°)	θ_{go} (°)	γ_{ow}, (mN m^{-1})	γ_{go}, (mN m^{-1})	C_s^i, (mN m^{-1})
Hexane	15.0	10.0	48.9	17.9	5.20
Decane	30.0	25.0/0[b]	50.1	23.22	−1.32
Dodecane	23.0	24.5	52.3	25.35	−5.65
Octane	N/M[c]	0[b]	49.82	22.52	−0.34

[a] The measured gas/water interfacial tension was 72 mN m^{-1}.
[b] Measured in a dry tube (two-phase conditions).
[c] N/M: not measured.

$$\psi_3 = \frac{\cos(\alpha + \theta_{go})}{\cos\alpha} \tag{8c}$$

and

$$B = (\pi/2 - \alpha)\tan\alpha \tag{8d}$$

where f_1 and f_2 are factors that range between 0 and 1 depending on the boundary conditions, where 0 corresponds to free and 1 corresponds to no-flow boundary conditions. Here f_1 represents the boundary condition at the oil/water interface, while f_2 represents the boundary condition at gas/oil interface. R is given by Eq. (4).

The total corner area including both water and oil is:

$$A_{cor} = r_{go}^2(\sin\omega(\cos\omega + \sin\omega\cot\alpha) - \omega) \tag{9}$$

and

$$\omega = \frac{\pi}{2} - \theta_{go} - \alpha \tag{10}$$

This expression is used to compute β and hence, from Eq. (7) the relationship between flow rate and potential gradient.

Zhou et al. [22] tested the validity of Eq. (8a) successfully by comparing it to the numerical results of Ransohoff and Radke [23]. Eq. (8a) was shown to be superior to either the hydraulic radius or thin film approximations. From experiments on square capillaries they showed that a free boundary condition at the gas/oil interface ($f_2 = 0$) and a no-flow boundary condition at the oil/water interface ($f_1 = 1$), when water is not flowing with oil, best fit Eq. (8a). In this paper we extend their work, using triangular capillaries, to study: (1) cases where oil and water flow together; (2) to test Eqs. (5) and (6) for oil layer formation; and (3) to study oil-wet systems.

3. Experiments

Experiments were performed with distilled water and *n*-hexane, *n*-octane, *n*-decane and *n*-dodecane as the oil phase. Interfacial tensions were measured using the 'pendant drop' technique [31]. To reproduce the experimental conditions, the oil was in contact with water for 24 h before measuring the oil/water interfacial tension. Contact angles were measured by performing capillary rise experiments [32] in circular glass capillaries of known radius, and using the literature values for density and the measured interfacial tensions. To measure the contact angles, the capillary tubes were prepared exactly the same way as the tubes for the flow experiments. Octane/air and decane/air contact angles were measured in a dry tube to represent two-phase conditions. Hexane/air, hexane/water, decane/air, decane/water, dodecane/air and dodecane/water contact angles were measured in a tube that was coated by a thin water film to represent three-phase conditions. Tables 2 and 3 show the measured values of interfacial tension, contact angle and the literature density and viscosity for the fluids used in the experiments [33].

Table 3
The viscosity and the density of the oils used in the experiments[a]

	μ (cp)	ρ (kg m^{-3})
Hexane	0.304	656.3
Decane	0.838	730.0
Dodecane	1.350	748.7
Octane	0.508	698.6
Water	0.9325	1000

[a] See reference [33].

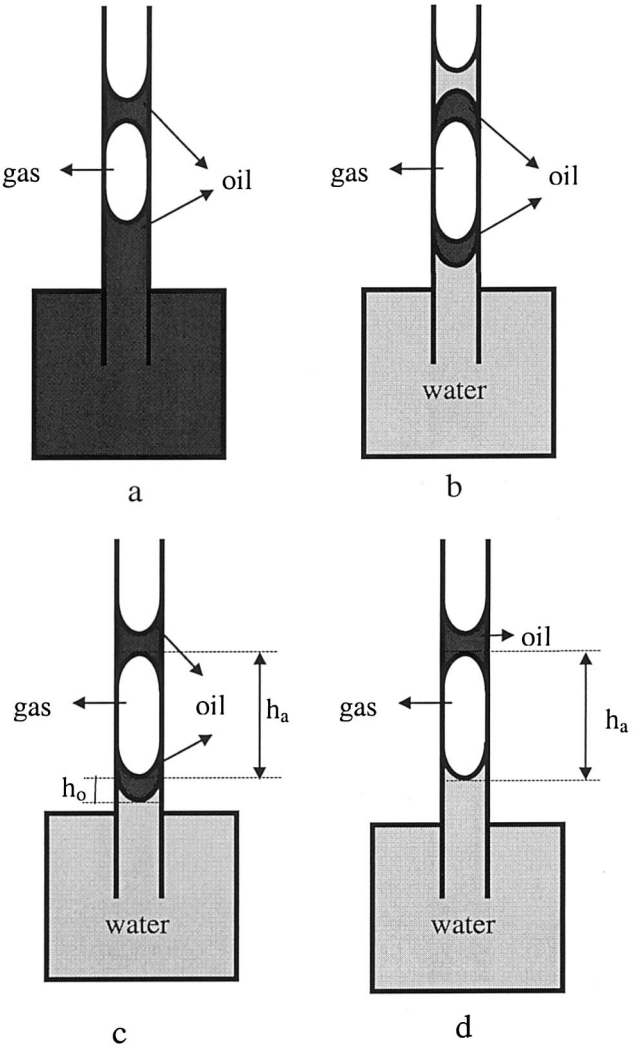

Fig. 3. Experimental setups in water-wet tubes. (a) Setup for the two-phase experiments. (b) Setup for the three-phase mobile water experiments. (c) Setup for the three-phase stationary water experiments. (d) Setup for the non-spreading three-phase experiments.

3.1. Two-phase experiments

Two-phase experiments were conducted to determine the boundary conditions at the gas/oil interface. As shown in Fig. 3, the setup and the procedures were similar for all experiments. For two-phase experiments a dry tube was filled with the oil phase, next an air bubble was allowed to enter the tube, then the air bubble was trapped with a blob of oil. The tube was held vertically and the drainage time for oil was measured (Fig. 3a). Three different tubes with side length of 0.4, 0.6 and 0.8 mm were used in the experiments.

3.1.1. Results of the two-phase experiments

For these two-phase experiments the theoretical value of β was obtained from the tables provided by Ransohoff & Radke [23]. Eq. (7) was used to compute the measured β. Knowing the length of the oil blob and the cross-sectional area of the tube, the volume of the oil blob was calculated. The flow rate, q_o, in Eq. (7) was found by dividing

the blob volume by measured drainage time. We then divided the flow rate by 3, since Eq. (7) applies for flow in a single corner, and our triangular tubes had three corners. If we assume that the oil flows under gravity with the gas phase stationary, the potential gradient is $\nabla\Phi = -(\rho_o - \rho_g)g$, where ρ_o and ρ_g are the densities of oil and gas and g is the acceleration due to gravity. Since the density of gas is very small compared to the oil density, ρ_g can be ignored.

The gas/oil capillary pressure for air to enter the tube for triangular cross-sections is [34],

$$P_{cgo} = \frac{\gamma_{go} F(\theta_{go})}{r_{cap}} = \frac{\gamma_{go}}{r_{go}} \quad (11)$$

$$F(\theta_{go}) = \frac{\theta_{go} + \cos^2\theta_{go} - \pi/6 - \sin\theta_{go}\cos\theta_{go}}{\cos\theta_{go} - \sqrt{\pi/6 - \theta_{go}\sin\theta_{go}\cos\theta_{go}}} \quad (12)$$

where, P_{cgo} is the gas/oil capillary pressure and r_{cap} is the inscribed radius of the capillary. Eq. (11) is used to find r_{go} in Eq. (7). We assume that P_{cgo} is fixed, and therefore the r_{go} is constant along the length of the air bubble.

Table 4 compares the theoretical and measured values of β. The value of β for free and no-flow boundary conditions for $\alpha = 30°$ and $\theta_{go} = 0°$ is 31.7 and 65.02, respectively [23]. The average β values obtained from 12 measurements for octane is 33.5 and for 14 measurements for decane is 32.7. The standard deviation of the data is 1 for octane and 0.7 for decane. The measured β values are between the free and no-flow boundary conditions, but are obviously closer to the free boundary condition with a difference of around 7.5%. Fig. 4 shows the measured drainage times for octane experiments performed in 0.8 mm tube compared with the predictions, assuming a free boundary condition. The results are similar for decane and for other tube sizes.

Table 4
Dimensionless resistance β for the two-phase flow experiments

	Measured		Literature[a]	
	Octane	Decane	Free B.C.	No flow B.C.
β	33.6 ± 1.0	32.7 ± 0.7	31.07	65.02

[a] See reference [23].

3.2. Three-phase experiments in water-wet tubes

3.2.1. Setup and procedure

Three-phase experiments were conducted to determine the boundary conditions at the gas/oil and oil/water interfaces and to investigate the existence of oil layers for non-spreading systems.

It is important for these experiments to make sure that the tube is completely water-wet. To do this, the tubes were cleaned with chromic acid and then washed thoroughly with distilled water. Then the tube was filled with water, next a blob of oil was introduced, then air was allowed to enter the tube and last the air was trapped with another blob of oil. For stationary water systems the tube was held vertically and the drainage time for oil was measured (Fig. 3c). For mobile water systems a blob of water was added at the top of the system, and then the drainage rates for both oil and water were measured (Fig. 3b). These experiments were conducted for tubes of side length 0.6 and 0.8 mm.

For non-spreading systems, air was trapped between water and oil. The height of the air bubble, h_a, at the point when oil drainage stopped was determined (Fig. 3d). In these experiments tubes with 1 mm side length were used.

3.2.2. Results for spreading systems

Hexane, which has a positive initial spreading coefficient, was the oil phase. Experiments were performed for two different cases: stationary and mobile water in the corners.

We analyze our experiments by finding values of r_{ow} and r_{go} in Eqs. (7) and (8a) that fit our measured flow rates for various interfacial boundary conditions. When the tube is horizontal, the gas/oil and oil/water radius of curvatures are equal and there is no-flow. When the tube is moved to the vertical position, the hexane forms layers between gas and water and these layers push the water into the corners. As a result the water flows slowly and the oil flows relatively fast.

While analyzing the results for the mobile water case, the oil/water radius of curvature, r_{ow}, that gave the observed water flow rate was computed from Eq. (7) for a range of values for β corresponding to different boundary conditions at the

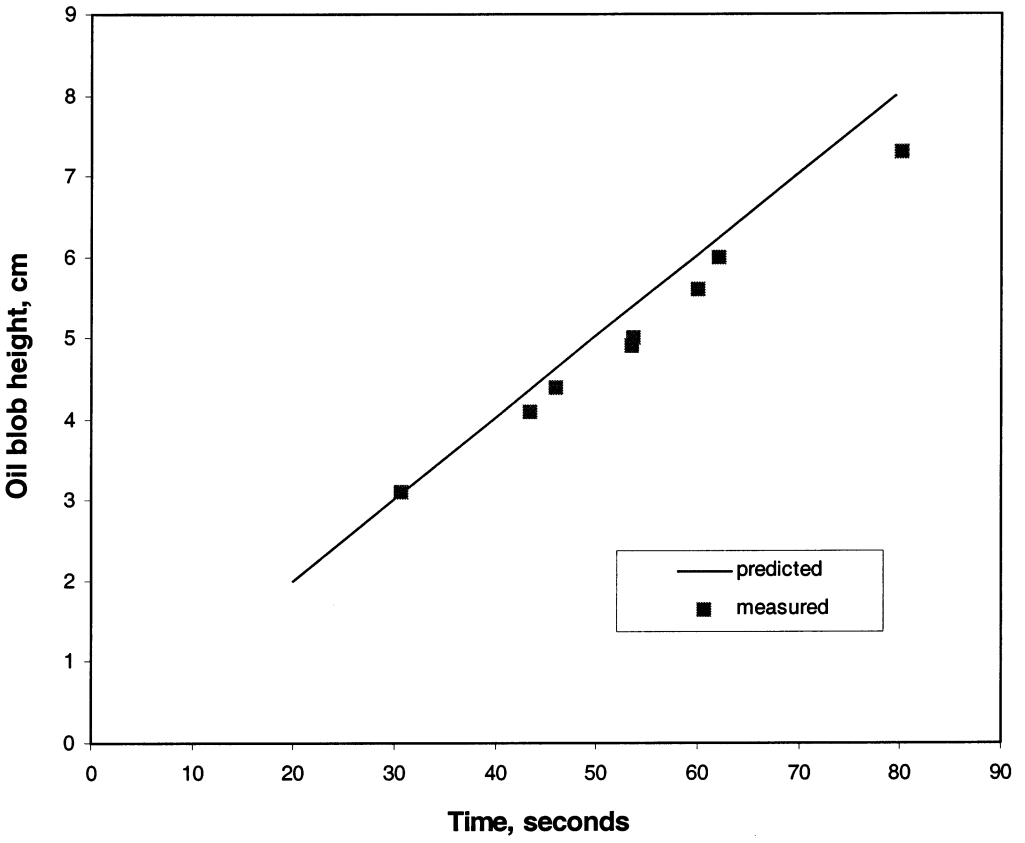

Fig. 4. Measured and predicted drainage times for two-phase flow for octane. The predicted curve assumes a free gas/oil boundary condition.

oil/water interface. The values of β were obtained from the tables in Ransohoff and Radke [23]. Since here we consider the flow of water, in Eq. (7) r_{ow} was substituted for r_{go}, μ_w for μ_o and q_w for q_o. We used Eq. (9) to find the corner area but with r_{ow} and θ_{ow} substituted for r_{go} and θ_{go} in Eqs. (9) and (10). The oil and water are assumed to be flowing freely under gravity. The potential gradient in Eq. (7) in this case is, $\nabla\Phi = -\rho_w g$ where ρ_w is the water density. For oil flow the potential gradient is $-\rho_o g$. We assume that the phase pressures are fixed and thus r_{ow} and r_{go} are constant along the tube.

The gas/oil radius of curvature, r_{go}, was calculated from Eq. (8a) using the measured oil flow rate, free boundary conditions at the gas/oil interface ($f_2 = 0$), as verified in the previous section, and various boundary conditions at the oil/water interface ($0 < f_1 < 1$) with the corresponding values of r_{ow}. Here f_1 was used as a fitting parameter to match the measured oil flow rate. The computed r_{go} is compared to the theoretical value, which is calculated by Eq. (11).

Table 5 compares the calculated value of r_{go} with the theoretical value of r_{go} for five experiments on the 0.8 mm tube. Excellent agreement between the theoretical and measured values is achieved for $f_1 \approx 0.5$ with an error around 2%. This shows that there is free boundary condition at the gas/oil interface, and at the oil/water interface the boundary condition is between free and no-flow boundary conditions when water is flowing with oil.

For the stationary water experiments, the theoretical r_{go} (Eq. (11)) was used to calculate r_{ow} for different boundary conditions at the oil/water in-

Table 5
Experimental results for the three-phase experiments with mobile water in 0.8 mm sided tubes[a,b,c]

r_{ow} (mm)	r_{go} (mm)
9.954×10^{-2}	1.464×10^{-1}
8.364×10^{-2}	1.374×10^{-1}
8.890×10^{-2}	1.417×10^{-1}
9.963×10^{-2}	1.461×10^{-1}
9.611×10^{-2}	1.467×10^{-1}
Average error = 2.1%	

[a] r_{ow} and r_{go} are compared to match the measured water and oil flow rates, respectively. f_1, which indicates the boundary condition at the oil/water interface, is fitted to match the theoretical r_{go}.
[b] Theoretical $r_{go} = 0.1446$ mm.
[c] $f_1 = 0.5$.

terface by solving Eq. (8a) with the known oil flow rate. Just like in the mobile water case, f_1 was used as a fitting parameter to match the measured oil flow rate. Again we assume oil flows freely under gravity with $\nabla\Phi = -\rho_o g$. The comparison of the measured and the theoretical r_{ow} values can be seen in Table 6. The theoretical values of r_{ow} were obtained by using capillary-gravity equilibrium at the point where oil starts to flow (the top of the air bubble). This is the smallest value of r_{ow} along the bubble, and represents the largest flow area for oil, which we assume dominates the overall flow rate. The equations used for this purpose are as follows:

$$P_{cow} = \frac{\gamma_{ow}}{r_{ow}} = P_o - P_w = P^*_{cow} + (h_a + h_o)(\rho_w - \rho_o)g \tag{13}$$

$$P^*_{cow} = \frac{\gamma_{ow} F(\theta_{ow})}{r_{cap}} \tag{14}$$

where P_{cow} is the oil/water capillary pressure, $F(\theta_{ow})$ is the same as Eq. (12) with θ_{ow} instead of θ_{go}. h_a and h_o are the gas bubble height and oil blob height, respectively (see Fig. 3c). The values of h_a and h_o were slightly different for each measurement. This analysis assumes a fixed value of r_{ow} controlled by capillary-gravity equilibrium. In reality r_{ow} changes along the air bubble. However, this simple analysis gives results that are virtually identical to a more detailed treatment where the flow rate is computed for varying r_{ow} [22,25].

The measured and theoretical values of r_{ow} agree with an average error of 3.2% for the 0.8 mm tube when a no-flow-boundary condition ($f_1 = 1$) is used at oil/water interface. In the smaller, 0.6 mm, tube the best results are obtained for $f_1 = 0.6$. These results show that for the stationary water case, there is approximately a no-flow boundary condition at the oil/water interface. This explains why the measured oil flow rates were higher when water was flowing than when it was stationary.

Once again we emphasize our approach—we use our measurements to find the boundary conditions to use in an empirical expression for flow rate. We observe oil layer drainage, and can cal-

Table 6
Experimental results for the three-phase experiments with stationary water[a]

Size = 0.8 mm ($f_1 = 1$)		Size = 0.6 mm ($f_1 = 0.6$)	
Theoretial r_{ow} (mm)	Measured r_{ow} (mm)	Theoretical r_{ow} (mm)	Measured r_{ow} (mm)
8.390×10^{-2}	8.983×10^{-2}	6.613×10^{-2}	7.144×10^{-2}
7.809×10^{-2}	8.212×10^{-2}	6.896×10^{-2}	6.827×10^{-2}
8.206×10^{-2}	8.248×10^{-2}	7.098×10^{-2}	6.850×10^{-2}
7.894×10^{-2}	8.086×10^{-2}	6.831×10^{-2}	6.844×10^{-2}
8.967×10^{-2}	9.092×10^{-2}	–	–
8.348×10^{-2}	8.158×10^{-2}	–	–
Average error = 3.2%		Average error = 2.9%	

[a] The theoretical value of r_{go} is used to find the oil flow rate, with r_{ow} computed to match the measurements. f_1 is fitted to match the theoretical r_{ow}, computed assuming gravity/capillary equilibrium.

culate the drainage rate with an analytical expression using physically reasonable boundary conditions.

3.2.3. Results for non-spreading systems

In this part of the study oil layer formation in non-spreading systems is investigated. Experiments were performed to determine the point where layer drainage stops using decane and dodecane to represent non-spreading oils. The measurements were used to test the relations given by Eqs. (5) and (6).

When the tube is held vertically, an oil layer does not always form. In non-spreading systems, the oil can form a lens in the capillary and there is a three-phase (oil/water/gas) contact line. In this case an oil layer is not present and the oil blob remains above the air bubble (Fig. 3d) without draining.

Eqs. (5) and (6) present a simple geometric argument for the formation of oil layers. r_{ow} at the top of the air bubble decreases with the height of the bubble, assuming capillary/gravity equilibrium. We use Eq. (13) to find r_{ow} with $h_o = 0$, and r_{go} is computed from Eq. (11). For small air bubbles r_{ow} is large, hence $R = r_{ow}/r_{go}$ may be larger than R_c and thus at the top of the bubble an oil layer may not form. For larger air bubbles r_{ow} is smaller, making $R < R_c$ and layer drainage is observed. We find the theoretical values of R_c for oil layer formation at the top of the air bubble using our measured contact angles. Experimentally we introduced air bubbles of different, decreasing heights and observe the height at which layer drainage first ceases. Using Eqs. (11) and (13) we determined a measured value of R_c.

As seen in Table 7, since decane is more spreading than dodecane, it has a higher value of R_c than dodecane. For both oils the theory over-predicts R_c with an error around 20 and 35%. This is not surprising, since the simple theory ignores the fluid arrangement in the vertical direction. Also the results are very sensitive to the values used for contact angle. However, note that oil layers are observed even for oils with negative spreading coefficients over a wide range of R.

Table 7
Comparison of the measured and theoretical critical radius of curvature ratios, R_c

	Measured R_c	Predicted R_c	Error (%)
Decane	0.863	1.110	22.25
Dodecane	0.623	0.964	35.37

3.3. Oil-wet systems

We performed two and three-phase experiments in oil-wet tubes. In two-phase experiments, we examined oil drainage in the presence of gas, and water drainage in the presence of oil. The flow rates were measured and compared to the corresponding systems in water-wet media. We also investigated the possible formation of water layers in the presence of three-phases in oil-wet systems.

3.3.1. Description of the system

Hexane was used as the oil phase. Contact angles were measured by capillary rise in oil-wet circular capillaries. The results are shown in Table 8.

3.3.2. Setup and procedure

The first step in these experiments is to make the tube oil-wet. For this purpose the tubes were exposed to a 20% crude (Thums, Long Beach, CA) and 80% octane mixture for 2 days and then washed thoroughly with octane. This has been demonstrated as a reliable method for rendering surfaces oil-wet [35], [36]. The experimental setup and procedure are similar to the experiments in water-wet capillaries (Fig. 5a and b), with the difference that now oil occupies the corners instead of water (Fig. 6). In two-phase experiments the tube is filled with oil and then

Table 8
Contact angle measurements in oil-wet tubes

Hexane-air, θ_{go} (°)	Hexane-water, θ_{ow} (°)	Water-air, θ_{gw} (°)
0	152	103

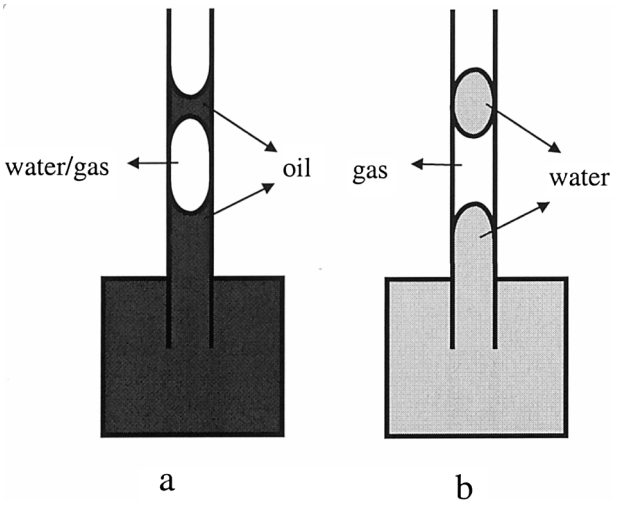

Fig. 5. Setup for the oil-wet system. (a) Two-phase oil flow in the presence of water or gas. (b) Three-phase water flow in the presence of gas.

either gas or water is introduced into the system. To examine the oil flow in the presence of gas, the gas is trapped with a blob of oil and then the drainage time for oil is measured (Fig. 5a). To examine the water flow in the presence oil, water is added to the system. The water blob moves downwards and the oil moves up. The rate at which water moves down is measured.

In three-phase experiments, the oil-wet tube has water in the center and oil in the corners. Then gas is introduced and then the gas is trapped with a blob of water (Fig. 5b). In this case oil occupies the corners and water and gas compete to occupy the center of the tube.

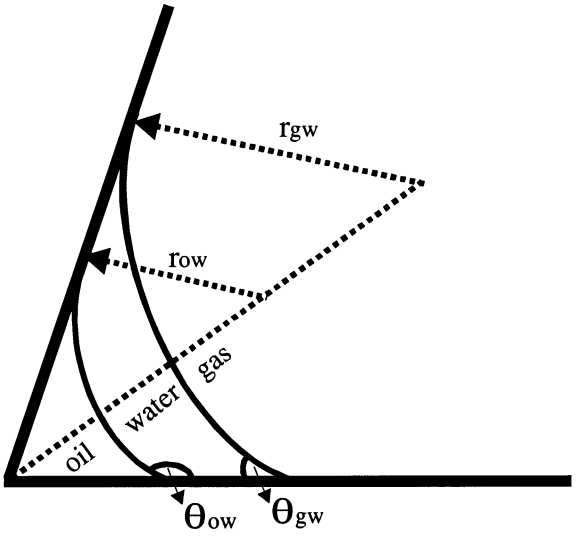

Fig. 6. Possible configuration of three phases in an oil-wet corner. While oil may form a wetting layer in the corner, we show that water layers are not possible.

3.4. Results of the oil-wet experiments

Oil flow in the presence of gas: The comparison of oil-wet and water-wet systems is illustrated in Fig. 7. In the presence of gas, oil drains in a water-wet medium through oil layers formed between water and gas. In oil-wet media oil layers reside in the corner regions of the capillary. The oil flow rates in both cases were similar. The behavior for the water-wet case was analyzed in the previous section. To analyze the oil-wet case we used $\nabla\Phi = -(\rho_o - \rho_g)g$. We find $\beta = 45 \pm 3$, which is higher than the β value measured in two-phase experiments ($\beta \approx 33$), but still fairly close to a free gas/oil boundary condition. The reason for the difference in the measured β values is that immobile crude oil still resided in the corners of the capillary, leaving a smaller flow area for hexane. When the tube was examined under a microscope the clogging of the corners could be seen directly.

Water flow in the presence of gas: The comparison of oil-wet and water-wet systems is illustrated in Fig. 8. Water drains in a water-wet medium through the layers formed in the corner regions of the capillary with a flow rate, $q_w = 5.7 \times 10^{-10}$ m^3 s^{-1}. To find β we used Eq. (7) with $\nabla\Phi = -\rho_w g$ and r_{gw}, q_w and μ_w substituted for r_{go}, q_o and μ_o. In Eqs. (9) and (10) r_{gw} and $\theta_{gw} = 0$ replaced r_{go} and θ_{go}. r_{gw} is found from Eq. (11) substituting γ_{go} and r_{go} by γ_{gw} and r_{gw}. Our measured $\beta = 37 \pm 2$ is consistent with a free gas/water boundary condition.

No drainage was observed in an oil-wet medium since there are no water layers formed between oil and gas. In oil-wet media, water forms layers if the following conditions are obeyed, as shown in Fig. 6 [24,35].

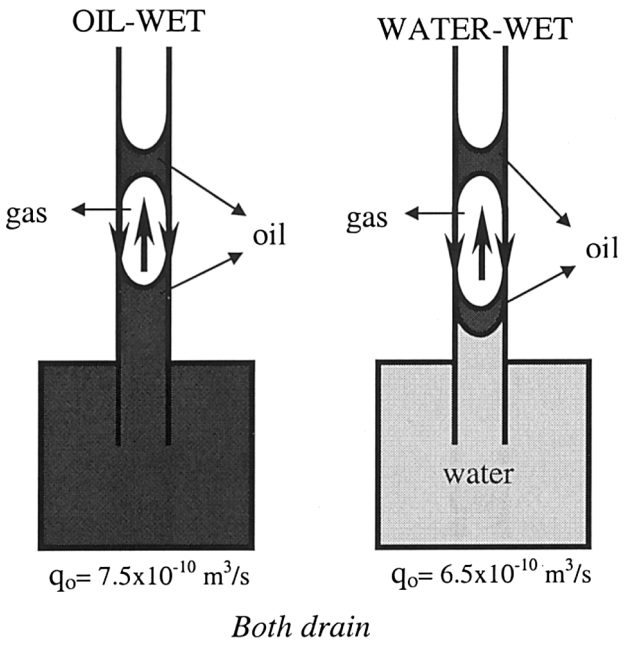

Fig. 7. Oil flow in the presence of gas in oil-wet and water-wet media. In both cases oil may form layers in the tubes, leading to similar drainage rates.

$$\theta_{ow} - \alpha > \frac{\pi}{2} \tag{15}$$

and

$$\theta_{gw} + \alpha < \frac{\pi}{2} \tag{16}$$

where $\alpha = \pi/6$ (30°) for a triangular capillary, and θ_{gw} is the gas/water contact angle.

Eq. (15) is satisfied since $\theta_{ow} = 152°$ (Table 8), and $152 - 30 > 90$, meaning that oil can form a wetting layer in our tubes. If we check Eq. (16) using $\theta_{gw} = 103°$, we see that $103 + 30 > 90$. Thus Eq. (16) is not satisfied and therefore water layers do not exist under these circumstances, as observed in the experiments. Note that since $\theta_{gw} > 90°$, gas is more wetting than water. Another way of understanding this is to note that the spreading coefficient of water on oil (C_{sw});

$$C_{sw} = \gamma_{go} - \gamma_{gw} - \gamma_{ow} \tag{17}$$

is -103 mN m^{-1}, which is very large and negative.

Water flow in the presence of oil: The comparison of oil-wet and water-wet systems is shown in Fig. 9. Water drains more slowly in presence of oil in a water-wet medium, than it does in an oil-wet medium. We computed β from Eq. (7) with $\nabla\Phi = -(\rho_w - \rho_o)g$. Since we consider two-phase oil/water flow, r_{ow} was substituted for r_{go}. The value of r_{ow} was found from Eq. (11), with γ_{ow} and r_{ow} replacing γ_{go} and r_{go}, respectively. To find the corner area r_{ow} and θ_{ow} are used in Eqs. (9) and (10) in place of r_{go} and θ_{go}. In the water-wet case, μ_w and q_w replace μ_o and μ_o in Eq. (7). In oil-wet tube $\beta = 60$, while in water-wet case $\beta \approx 1000$. The theoretical values of β for the oil-wet case ($\theta_{ow} = 152°$) are 54 and 116 for free and no-flow boundary conditions, respectively. For the water-wet case ($\theta_{ow} = 15°$), β is 34 and 74 for free and no-flow boundaries [23]. For the oil-wet tube the results are close to a free boundary condition, while in the water-wet case, the water flow is slower than would be expected for even a no-flow boundary. These experiments study counter-current flow, where two viscous fluids, oil and water, are flowing in opposite directions. This explains why the measured values of β can be higher than for two-phase liquid/gas flow. For the water-wet tube the upwards movement of

oil considerably hinders the downwards drainage of water. Since oil is less viscous than water, it acts as a better lubricant in the corners, resulting in a lower β for the oil-wet case than for the water-wet case. A full treatment of this problem requires a consideration of coupling between phases, where the potential gradient in one phase affects the flow of another phase. This topic has been discussed by other authors, for instance Kalaydijan [37], but is beyond the scope of this work.

4. Remarks

We found the boundary conditions for oil/water and gas/oil interfaces. There is a free boundary condition at the gas/oil interface. The boundary condition at the oil/water interface is a no-flow boundary for stationary water and is between no-flow and free boundary conditions when water is also flowing. We investigated the existence of oil layers and experimentally showed that there is a critical radius of curvature ratio when oil layers collapse. We compared oil-wet and water-wet media in terms of oil and water drainage rates. However, despite the simple nature of the experiments, there are still some complex issues, in particular the dependence of the flow direction of one phase on the flow of another, the impact of clogging by crude oil during wetability alteration, and the influence of three-dimensional geometry on oil layer formation.

With some limitations, we now have calibrated and verified analytical expressions for flow rate and layer formation in a single pore. These can be input into a model with a three-dimensional network of pores to predict macroscopic properties, such as relative permeability. To illustrate this approach simply, we will derive the relative permeability of a single tube and compare it with experimental results on a sandpack.

5. Relative permeability example

Oil relative permeability can be calculated for a single tube by using the expressions for layer conductance with the appropriate boundary conditions discussed in this paper. The conductance of a tube completely filled by a single phase is given by assuming a Poiseuille-type relationship:

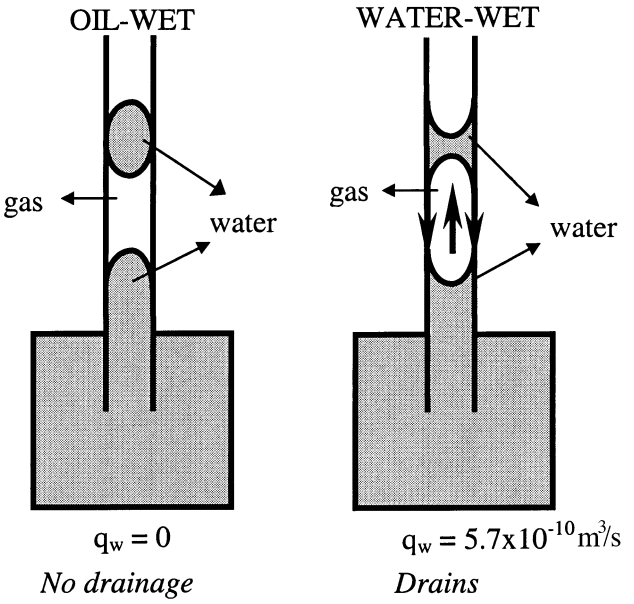

Fig. 8. Water flow in the presence of gas in oil-wet and water-wet media. In the oil-wet tube, water layers do not form and no water flow is observed.

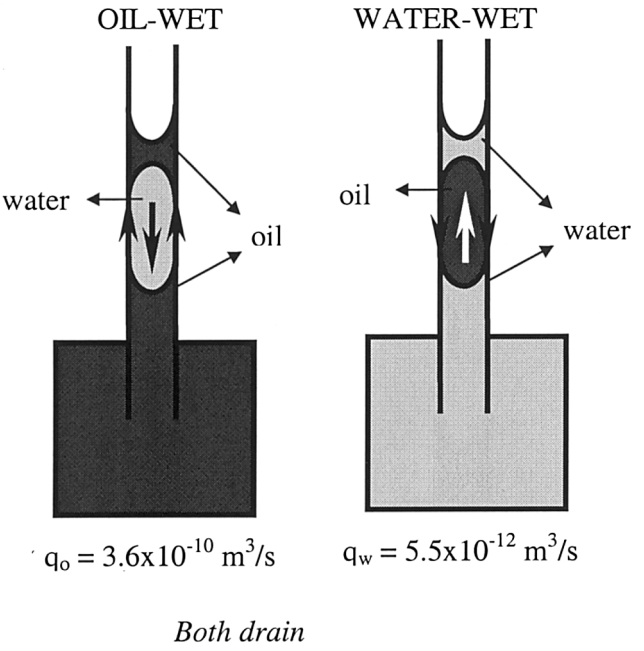

Fig. 9. Water flow in the presence of oil in oil-wet and water-wet media. In both cases wetting layers are present. In this example we have counter-current flow with viscous fluids, oil and water, moving in opposite directions. This significantly decreases the flow rate in the water-wet tube.

$$q = -g\nabla\Phi \tag{18}$$

where g is the conductance and is closely approximated as follows [21],

$$g = \frac{3r_{cap}^2 A_t}{20\mu} \tag{19}$$

where A_t is the total cross sectional area of the capillary.

We will consider three-phase flow in a water-wet tube. The oil layer conductance for each corner can be calculated by using the relation for β given by Zhou et al. [22] (Eq. (8a)). The conductance $g°$ from Eqs. (7) and (18) is simply,

$$g^\circ = \frac{r_{go}^2 A_{cor}}{\beta\mu_o} \tag{20}$$

The relative permeability of the tube, k_{ro}, is the ratio of $g°$ to g times the number of corners that the capillary has (three for a triangle), i.e. $k_{ro} = 3g°/g$. The oil area in the corner A_o,

$$A_o = A_{cor} - A_w \tag{21}$$

where, A_{cor} is given by Eq. (9) and A_w is calculated by replacing r_{go} and θ_{go} in Eqs. (9) and (10) with r_{ow} and θ_{ow}. The oil saturation $S_o = 3A_o/A_t$.

Figs. 10 and 11 compare the oil relative permeability measured by Sahni et al. [38] in three-phase gravity drainage experiments, with the single capillary tube relative permeability calculations. The boundary condition determined in the experiments for oil and water both flowing ($f_1 = 0.5$ and $f_2 = 0$) and the contact angles measured for decane ($\theta_{ow} = 30°$, $\theta_{go} = 25°$) were used for the calculations. Octane contact angles (θ_{ow}, θ_{go}) were assumed to be zero. The water saturation S_w was assumed to be 10% which is the same as in the experiments at low S_o.

First compare the experimental results in Figs. 10 and 11. Both experiments were performed on similar water-wet sandpacks—the only difference was the oil used. In Fig. 10 (octane) very low oil saturations were reached, with $k_{ro} \approx S_o^2$ for $S_o \leq 0.15$. In contrast in Fig. 11 (decane) k_{ro} falls sharply at $S_o \approx 0.1$.

The computation of relative permeability in a single triangular capillary clearly will not match the experimental data—in particular, our calculation assumes that all pores have gas filling their centers, whereas in reality some pores will also be oil and water filled. Furthermore, the complex topology of a real system is ignored. However, the key qualitative differences between Figs. 10 and 11 are readily explained from an analysis in a single tube. In the octane experiment, oil layers are present down to very low saturation. If $\theta_{go} = \theta_{ow} = 0$, $S_o = 0$ when octane layers are no longer present. The $k_{ro} \approx S_o^2$ form of the relative permeability is a direct consequence of layer drainage. S_o is proportional to the cross-sectional area of oil in a pore. The flow rate is approximately proportional to area squared, and hence $k_{ro} \approx S_o^2$. This behavior is evident in the calculated curve in Fig. 10 when the slope on the log–log plot is approximately 2. A more rigorous analysis of the functional form for k_{ro} in a single tube based on Eq. (8a) is provided by Zhou et al. [22]. That the single tube computation over-estimates k_{ro} by over an order of magnitude is not surprising, since the tortuosity of the porous medium is ignored. What is remarkable in the experiments is that very low values of S_o are reached and that k_{ro} is consistent with layer drainage. The same $k_{ro} \approx S_o^2$ behavior also been observed for hexane [38], and for spreading oils in water-wet bead packs [39] and in sandstone [40].

Oil layers for decane collapse during the displacement leading to trapping of oil, since $\theta_{go} \neq \theta_{ow} \neq 0$ and the layer drainage regime down to low S_o is not observed in the experiments, Fig. 11. The simple geometric argument for layer formation, combined with Eq. (8a) for β, captures qualitatively the same behavior as the experiments and shows a sharp drop in k_{ro} at around $S_o = 0.1$.

Using a more realistic geometric model of the pore space, together with the expressions presented here for conductance, it is hoped that network modeling could provide a reliable prediction of three-phase relative permeability. Fenwick and Blunt [14], predicted k_{ro} using network modeling and captured some of the generic features of three-phase experiments. However, a simpler expression than Eq. (8a) was used to compute oil layer conductance, and no attempt was made to match the experimental pore size distribution and topology.

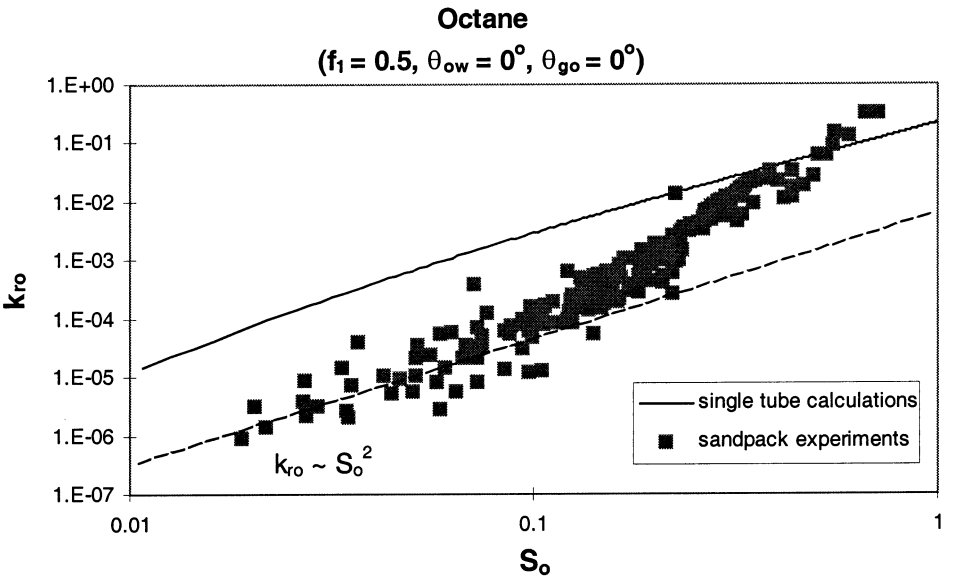

Fig. 10. The comparison of sand-pack experiments of Sahni et al. [38] with single tube calculations for octane. The dashed line $k_{ro} \approx S_o^2$ is a fit through the experimental points at low saturation.

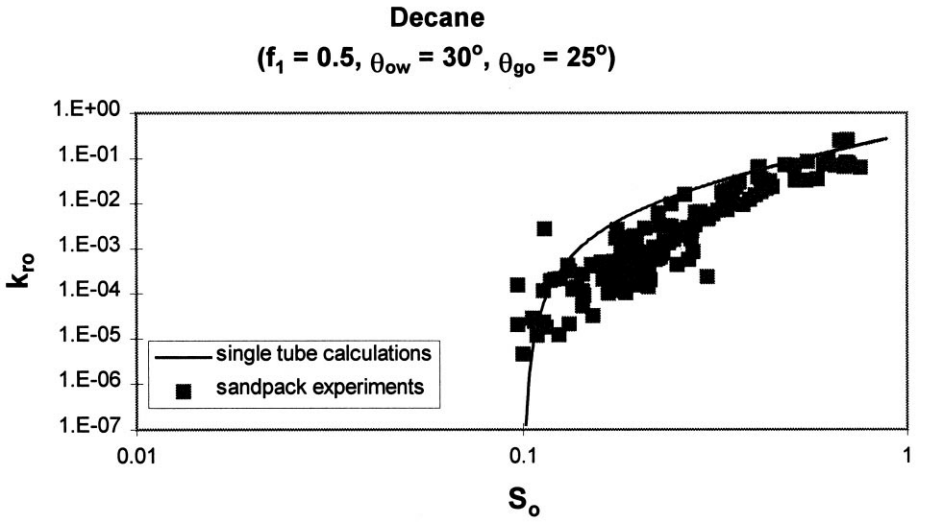

Fig. 11. The comparison of sand-pack experiments of Sahni et al. [38] with single tube calculations for decane.

6. Conclusions

The aim of this work was twofold. First to perform a comprehensive series of two and three-phase flow experiments in water-wet and oil-wet angular capillaries. Second, to interpret the results using theoretical expressions for flow rate and layer formation for input into pore scale network models. The analysis revealed some subtleties in even these conceptually simple experiments. We showed that the flow rate of wetting layers is very sensitive to the flow direction and viscosity of the phase occupying the center of the tube. Three-dimensional computations of the stability of three-phase contact lines are necessary to obtain more than an approximate indication of layer formation. Last, using crude oil to change wetability also alters the pore structure, since immobile oil components clog up the corners.

Despite the complications, the following conclusions can be made.

1. A free boundary condition at gas/oil and gas/water interfaces allowed good agreement between measured and theoretical values of flow rate.
2. In three-phase experiments, the results were consistent with a no-flow boundary condition at the oil/water interface if water was not moving, and an intermediate condition between a free and a no-flow boundary if water was flowing with oil.
3. Oil layers could form for non-spreading oils. The critical ratio of interfacial curvatures at which layers would first not be present was measured and the results approximately agreed with the expression derived by Fenwick and Blunt [13].
4. In oil-wet systems, layers of the intermediate-wet phase (water or gas) do not form, consistent with a simple geometric argument. The flow rate of oil as the most wetting phase is consistent with a free gas/oil boundary condition, as found for water-wet media.
5. Using the expression for layer conductance and the geometric argument for oil layer existence, the qualitative features of drainage experiments in sandpacks could be explained. The characteristic behavior of the oil relative permeability at low saturation for a spreading system, $k_{ro} \approx S_o^2$, is a direct consequence of oil layer drainage. For a non-spreading oil the onset of layer collapse predicted in a single tube matched the observed drop in k_{ro} at $S_o \approx 0.1$.

Acknowledgements

We thank David Di Carlo for experimental assistance and Akshay Sahni for providing the data for Figs. 10 and 11. We gratefully acknowledge financial support from the Stanford University Gas Injection Affiliates Program (SUPRI-C) and DOE under Grant No. DE-FG22-96BC14851.

Appendix A. Nomenclature

A_{cor}	area of oil and water in a corner (m^2)
A_t	total cross sectional area of the capillary (m^2)
C_{so}	spreading coefficient for oil (mN m^{-1})
C_{sw}	spreading coefficient for water (mN m^{-1})
f_1	parameter to define boundary condition at oil/water interface
f_2	parameter to define boundary condition at gas/oil interface
h_a	air bubble height in capillary tube (m)
h_o	oil height in the capillary tube
g	total conductance for single phase (m^3 s N^{-1})
$g°$	conductance of oil in one corner (m^3 s N^{-1})
k_{ro}	oil relative permeability
P_{cgo}	gas/oil capillary pressure
P_{cow}	oil/water capillary pressure
q	flow rate (m^3 s^{-1})
R	radius of curvature ratio
R_c	critical radius of curvature ratio
r_{cap}	inscribed radius of the capillary (m)
r_{ow}	oil/water radius of curvature (m)
r_{go}	gas/oil radius of curvature (m)
r_{gw}	gas/water radius of curvature (m)
S	saturation
S_{or}	residual oil saturation

Greek symbols

α	half angle of the corner (rad)
β	dimensionless resistance
γ_{go}	gas/oil interfacial tension (mN m^{-1})
γ_{gw}	gas/water interfacial tension (mN m^{-1})
γ_{ow}	oil/water interfacial tension (mN m^{-1})
μ	viscosity (cp)
$\nabla\Phi$	potential gradient (N m^{-3})
θ_{go}	gas/oil contact angle (rad)
θ_{gw}	gas/water contact angle (rad)
θ_{ow}	oil/water contact angle (rad)

Subscripts

g	gas
o	oil
w	water

Superscripts

i	initial

References

[1] F.A.L. Dullien, Porous Media: Fluid Transport and Pore Structure, Academic Press, San Diego, 1992.
[2] H.L. Stone, J. Pet. Technol. 20 (1970) 214.
[3] M.J. Oak, Three-phase relative permeability of water-wet Berea, in: Proceedings of the SPE/DOE Symposium on Enhanced Oil Recovery, Society of Petroleum Engineers, Tulsa, OK, 1990, SPE 20183.
[4] G.R. Jerauld, Soc. Pet. Eng. Reserv. Eng. 12 (1997) 66.
[5] J.M. Dumoré, R.S. Schols, Soc. Pet. Eng. J. 14 (1974) 437.
[6] D. Zhou, M.J. Blunt, J. Contam. Hydrol. 25 (1997) 1.
[7] A. Kantzas, I. Chatzis, F.A.L. Dullien, Enhanced oil recovery by inert gas injection, in: Proceedings of the SPE/DOE Symposium on Enhanced Oil Recovery, Society of Petroleum Engineers, Tulsa, OK, 1988, SPE 17379.
[8] P.E. Øren, J. Billiote, W.V. Pinczewski, Soc. Pet. Eng. Form. Eval. 7 (1992) 78.
[9] Chatzis, I., Kantzas, A., F.A.L. Dullien, On the investigation of gravity assisted inert gas injection using micromodels, long Berea sandstone cores, and computer assisted tomography, in: Proceedings of the Annual Technical Conference and Exhibition of the Society of Petroleum Engineers, Society of Petroleum Engineering, Houston, TX, 1988, SPE 18284.

[10] A.A. Keller, M.J. Blunt, P.V. Roberts, Transp. Porous Media 26 (1997) 277.
[11] W.E. Soll, M.A. Celia, J.L. Wilson, Water Resour. Res. 29 (1993) 2963.
[12] M. Dong, E.A.L. Dullien, I. Chatzis, J. Colloid Interface Sci. 172 (1995) 21.
[13] D.H. Fenwick, M.J. Blunt, Soc. Pet. Eng. J. 3 (1998) 86.
[14] D.H. Fenwick, M.J. Blunt, Adv. Water Resour. 21 (2) (1998) 121.
[15] P.E. Øren, J. Billiote, W.V. Pinczewski, Pore-scale network modeling of waterflood residual oil recovery by immiscible gas flooding, in: Proceedings of the Improved Oil Recovery Symposium, Society of Petroleum Engineers, Tulsa, OK, SPE 27814.
[16] W.E. Soll, M.A. Celia, Adv. Water Resour. 16 (1993) 107.
[17] V. Mani, K.K. Mohanty, Soc. Pet. Eng. J. 3 (1998) 238.
[18] P.E. Øren, V.W. Pinczewski, The effect of wetability and spreading coefficients on the recovery of waterflood residual oil by miscible gas flooding, in: Proceedings of the Annual Technical Conference and Exhibition of the Society of Petroleum Engineers, Society of Petroleum Engineers, Washington D.C., SPE 24881.
[19] D. Zhou, M.J. Blunt, J. Pet. Sci. Technol. 20 (1998) 203.
[20] O. Vizika, J.M. Lombard, Soc. Pet. Eng. Reserv. Eng. 11 (1996) 54.
[21] P.E. Øren, S. Bakke, O.J Arntzen, Soc. Pet. Eng. J. 3 (1998) 324.
[22] D. Zhou, M.J. Blunt, F.M. Orr Jr., J. Colloid Interface Sci. 187 (1997) 11.
[23] T.C. Ransohoff, C.J. Radke, J. Colloid Interface Sci. 121 (1988) 392.
[24] P.E. Øren, W.V. Pinczewski, Transp. Porous Media 20 (1995) 105.
[25] M.J. Blunt, D. Zhou, D.H. Fenwick, Transp. Porous Media 20 (1995) 77.
[26] L.J.J Catalan, F.A.L. Dullien, I. Chatzis, Soc. Pet. Eng. Adv. Technol. Ser. 2 (1994) 140.
[27] F.J. Kalaydijan, J.C. Moulu, O. Vizika, P.K. Munkerud, Three-phase flow in water-wet porous media: determination of gas/oil relative permeabilities under various spreading conditions, in: Proceedings of the Annual Technical Conference and Exhibition of the Society of Petroleum Engineers, Society of Petroleum Engineers, Houston, TX, SPE 26671.
[28] H. Skurdal, O. Hustad, T. Holt, Oil recovery by gravity drainage durind gas injection, in: Proceedings of the European Symposium on Improved Oil Recovery, Vienna, Austria, 1995.
[29] O. Vizika, Effect of spreading coefficient on the efficiency of oil recovery with gravity drainage, in: Proceedings of the Symposium on Enhanced Oil Recovery, National Meeting of the American Chemical Society, Denver, CO, 1993.
[30] R. Lenormand, C. Zarcone, Role of roughness and edges during imbibition in square capillaries, in: Proceedings of the Annual Technical Conference and Exhibition of the Society of Petroleum Engineers, Society of Petroleum Engineers, Houston, TX, 1984, SPE 13264.
[31] A.A. Adamson, Physical Chemistry of Surfaces, Wiley, New York, 1990.
[32] N. Rashidnia, R. Balasubramaniam, D. Del Signore, AICHE J. 38 (1992) 615.
[33] R.C. Weast, M.J. Astle (Eds.), Handbook of Chemistry and Physics, 62nd ed., CRC, Boca Raton, Florida, 1981–1982.
[34] J. Legait, J. Benoit, Colloid Interface Sci. 96 (1983) 28.
[35] D.A. Di Carlo, A. Sahni, M.J. Blunt, The effect of wetability on three-phase relative permeability, in Proceedings of the Annual Technical Conference and Exibition of the Society of Petroleum Engineers, Society of Petroleum Engineers, New Orleans, LA, 1998, SPE 49317.
[36] J.S. Buckley, Y. Liu, X. Xie, N.R. Morrow, Soc. Pet. Eng. J. 2 (1997) 107.
[37] F. Kalaydijan, Transp. Porous Media 3 (1990) 215.
[38] A. Sahni, J. Burger, M.J. Blunt, Measurement of three phase relative permeability during gravity drainage using CT scanning, in: Proceedings of the SPE/DOE Improved Oil Recovery Symposium, Society of Petroleum Engineers, Tulsa, OK, 1998, SPE 39655.
[39] A.S. Grader, D.J. O'Meara Jr., Dynamic displacement measurements of three-phase relative permeabilities using three immiscible liquids, in: Proceedings of the Annual Technical Conference and Exhibition of the Society of Petroleum Engineers, Society of Petroleum Engineers, Houston, TX, 1988, SPE 18293.
[40] P. Naylor, N.C. Sargent, A.J. Crosbie, A.P. Tilsed, S.G. Goodyear, Gravity drainage during gas injection, in: Proceedings of the European Improved Oil Recovery Symposium, Vienna, Austria, 1995.